European Journal of
Nuclear
Medicine

Original article

# In vitro validation of a simple tomographic technique for estimation of percentage myocardium at risk using methoxyisobutyl isonitrile technetium 99m (sestamibi)

Michael K. O'Connor, Thomas Hammell, and Raymond J. Gibbons

Department of Diagnostic Radiology and Division of Cardiovascular Diseases and Internal Medicine, Mayo Clinic, Rochester, MN 55905, USA

Received May 9, 1989 and in revised form July 31, 1989

**Abstract.** With the advent of technetium 99m-labeled myocardial blood flow agents, there is a need for a simple technique for quantitation of infarcted or jeopardized myocardium (IM). This study provides an in vitro validation of a simple technique based upon the analysis of three short-axis slices through the heart following emission computed tomography. All acquisitions were performed using a static cardiac phantom containing pertechnetate Tc 99m. Activity in the phantom was adjusted so that the count density and myocardial-to-background ratio were comparable to those observed in patients. Plastic insets (range of sizes = 4%–72% of myocardium) were used to simulate transmural infarctions. Eighteen studies were acquired, each over 180° into a 64 × 64 matrix. Data were reconstructed using a Ramp Hanning filter with cut off at 0.7 times the Nyquist frequency. Short-axis slices of the myocardium were then generated, and representative apical (A), mid-ventricular (MV), and basal (B) slices were selected. For each slice, a circumferential profile was generated, and the average radius ($R$) was measured. The fraction ($F$) of the profile falling below a threshold value was considered to represent IM. Total IM was given by $\%\ IM = 100 \times (R_B F_B + R_{MV} F_{MV} + 0.67 R_A F_A)/(R_B + R_{MV} + 0.67 R_A)$, where the subscripts to R and F refer to the relevant short-axis slices. For a threshold set at 60% of peak, measured IM agreed closely with true IM ($R^2 = 0.98$, measured IM = 1.01 × true IM − 1.35). Measurement of % IM was not distorted by variations in slice radius or in slice selection. Maximum error in % IM occurred with a change in location of the infarct (approximately 4% for opposing walls). This technique permits rapid and accurate assessment of % IM with $^{99m}$Tc-labeled myocardial blood flow agents.

*Key words:* SPET – Infarct size – Cardiac phantom

**Eur J Nucl Med (1990) 17:69–76**

*Offprint requests to:* M.K. O'Connor

## Introduction

Over the past 10 years, many investigators have shown that single photon emission computed tomography (SPET) with thallous Tl 201 chloride can permit accurate measurement of total myocardial mass (Holman et al. 1983; Narahara et al. 1987) and myocardial infarct size (Prigent et al. 1986; Johnson et al. 1987; Weiss et al. 1983; Tamaki et al. 1982; Keyes et al. 1981). The use of thrombolytic agents and percutaneous transluminal angioplasty (PTCA) for acute therapy of myocardial infarction has provided a strong impetus for the development of quantitative methods to assess infarct size. Infarct size with SPET using $^{201}$Tl has been used as an endpoint in several clinical trials of thrombolytic therapy (Ritchie et al. 1984; DeCoster et al. 1985). However, such measurements are generally only feasible after intervention; assessment of the myocardium at risk before intervention is generally precluded by the time required to perform SPET imaging, the rapid redistribution of thallium 201, and the problem of reactive hyperemia following coronary reperfusion (Granato et al. 1986; Okada and Pohost 1984). Many of the commonly available indices, such as the patient's ECG, cardiac output, left ventricular end-diastolic pressure, and coronary anatomy cannot be used to predict accurately the size of the myocardium at risk (Feiring et al. 1987). Furthermore, while there is a good inverse linear relationship between the final left ventricular ejection fraction (LVEF) and the size of the myocardium at risk in the absence of reperfusion (Feiring et al. 1987; Schneider et al. 1985), this does not apply to the acute LVEF (Feiring et al. 1987).

With the recent introduction of sestamibi Tc 99m (methoxyisobutyl isonitrile Tc 99m), it is now feasible to assess the myocardium at risk prior to acute intervention. Like thallium 201, sestamibi Tc 99m is rapidly cleared from the blood and accumulates in normal myocardium in direct proportion to blood flow (Okada et al. 1988). Unlike thallium 201, sestamibi has a very slow

washout from the myocardium with minimal redistribution (Okada et al. 1988). As a result, delayed images obtained several hours post-injection provide information on the status of the myocardium before intervention (Wackers et al. 1989). A post-intervention scan can then be used to assess the efficacy of intervention. Clearly, for such applications, the quantitation of the percentage of the myocardium at risk is vital. Preliminary studies in dogs have shown that sestamibi Tc 99m can be used with SPET imaging to quantitate regional myocardial perfusion (Li et al. 1988). The purpose of this study is to describe and validate in a phantom model a simple, practical technique for quantitating the percentage of hypoperfused myocardium following the administration of $^{99m}$Tc-labeled radiopharmaceuticals.

## Materials and methods

*Cardiac phantom.* All studies were performed using the commercially available phantom shown in Fig. 1 (Model RH-2, Capintec, New Jersey). This consists of a body 30 cm wide and 20 cm thick containing a Teflon rod to simulate the thoracic vertebrae and two compartments containing wood powder to simulate the lungs. The "heart" consists of a right and left ventricle with separate compartments for the blood pool and myocardium. Plastic pieces were inserted into the myocardial compartment to simulate infarcted or jeopardized myocardium (IM). The volume of each plastic piece was determined by measuring the volume of water it displaced. Myocardial volume was 182 ml, and the volume of the IM varied from 7 to 130 ml, representing 3.8%–71.4% of myocardial mass. A total of 18 studies were performed with this phantom using pertechnetate Tc 99m. An additional 3 studies were performed using thallous Tl 201 chloride for comparison with their equivalent $^{99m}$Tc study. Figure 2 indicates the size of the myocardial defect present in each study and its anatomical location. Studies 17 and 18 contained "subendocardial infarctions"; in all other studies, the defects simulated transmural infarctions. Some infarct locations used in this project are unlikely to occur in clinical practice but were included so that the effects of diametrically opposed lesions on estimation of % IM could be studied.

*Cardiac activity.* In order to determine the appropriate activity to be placed in the myocardium and surrounding background, ten studies of patients with acute myocardial infarction were examined. For each study, the patient had received 20–30 mCi of sestamibi Tc 99m at rest before thrombolytic therapy. Tomographic acquisition was performed 1–6 h later using a standard large field-of-view gamma camera (Elscint 409, Israel) equipped with a low-energy, all-purpose collimator. Using a $64 \times 64$ matrix, 30 images were acquired for 40 s per image every 6° over 180°, beginning at 45° RAO and ending at 45° LPO. For analysis of myocardial-to-background activity, the 45° LAO image was selected and regions of interest (ROI) drawn around the myocardium and background adjacent and lateral to the myocardium. Care was taken to exclude any small-bowel activity in the field of view. Background ROI was adjusted to the same size as the myocardial ROI and the myocardial-to-background ratio obtained. This was $1.64 \pm 0.17$ (mean $\pm$ standard deviation) in ten studies. The background-corrected myocardial activity was $17781 \pm 7463$ counts per 40 s in a 45° LAO view. Since some degree of myocardial infarction was present in

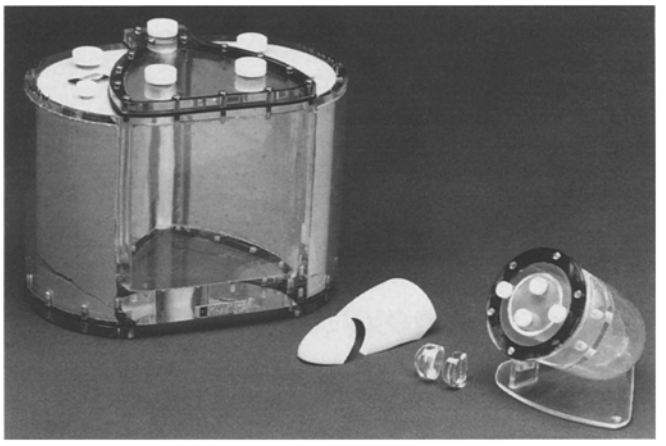

**Fig. 1.** The various components of the cardiac phantom. The simulated lungs and thoracic vertebrae can be seen in the phantom. The heart contains a right and left ventricle. A variety of insets (simulating jeopardized or infarcted myocardium) can be placed in the left ventricular myocardium

| Study number | Infarcted myocardium, % | Location of "infarct" in myocardium | | | |
|---|---|---|---|---|---|
| | | Horizontal long axis | | Vertical long axis | |
| | | Superior | Inferior | Medial | Lateral |
| 1 | 0 | | | | |
| 2 | 4.4 | | | | |
| 3 | 3.8 | | | | |
| 4 | 3.8 | | | | |
| 5 | 12.1 | | | | |
| 6 | 12.1 | | | | |
| 7 | 18.7 | | | | |
| 8 | 18.7 | | | | |
| 9 | 30.8 | | | | |
| 10 | 30.8 | | | | |
| 11 | 37.4 | | | | |
| 12 | 37.4 | | | | |
| 13 | 49.5 | | | | |
| 14 | 49.5 | | | | |
| 15 | 71.4 | | | | |
| 16 | 71.4 | | | | |
| 17 | 19.2 | | | | |
| 18 | 19.2 | | | | |
| 19* | 0 | | | | |
| 20* | 0 | | | | |
| 21* | 37.4 | | | | |

**Fig. 2.** Diagrammatic representation of the left ventricular myocardium, showing the location and size of the selected 'transmural' (in *black*) and 'subendocardial' (in *grey*) defects in the 21 studies. Note that studies 1–18 were acquired using $^{99m}$Tc. Study 19 was acquired using $^{201}$Tl (80 keV peak only), and studies 20–21 using $^{201}$Tl (80 and 170 keV peaks)

all studies, these results represent an underestimation of the values that would be obtained in normal myocardium.

Activity in the cardiac phantom was 2 mCi $^{99m}$Tc in the background cavity and 1.5 mCi $^{99m}$Tc in the myocardium (for a "normal" myocardium). No activity was placed in the left ventricle. For an 8-s image acquisition in the 45° LAO position, this gave a myocardial-to-background ratio of 1.86 and corrected myocardial activity of 21400 counts per 8 s. With the introduction of myocardial defects, the activity in the myocardium was reduced in proportion to the size of the defect. For the three studies employing $^{201}$Tl, identical amounts of activity were placed in the myocardium and background as compared with the equivalent $^{99m}$Tc study.

*Data acquisition and processing.* For each of the 21 phantom studies, the selected defect was placed in the myocardium and the myocardium and surrounding background filled with the appropriate activity as described above. The phantom was agitated for 5 min to ensure uniform mixing of the isotope in the appropriate compartments. The phantom was orientated on the SPET imaging table in a manner similar to the patient's position for clinical studies. Tomographic acquisition was then performed using a rectangular large field-of-view gamma camera (Elscint 609, Israel). Images were acquired for 8 s per image using similar acquisition parameters to those described above for patient studies. One-pixel thick transaxial slices were generated by filtered back projection using a Ramp Hanning filter cut off at 0.7× the Nyquist frequency. From the transaxial slices, horizontal and vertical long-axis slices were generated for each study. From these the limits of the myocardium were visually determined and short-axis slices generated between these limits. If no apical activity was present, the location of the apex was estimated from the midventricular long-axis slice. No attenuation correction was applied to the data.

*Measurement of percentage infarcted or jeopardized myocardium – total slice technique.* The measurement of myocardial mass is based upon the sum of cylinders method (i.e., the myocardium can be considered as a series of cylinders of radii equal to the average radii of the short-axis slices and height equal to the thickness of the short-axis slices). If we consider a single short-axis slice of mean radius $R$, myocardial thickness $T$, and height $H$, then the volume of this slice is given by the equation

$$V=\pi H(R+T/2)^2-\pi H(R-T/2)^2 \\ =2\pi RHT \quad (1)$$

If we assume that myocardial thickness is a constant, then

$$V=kR, \quad \text{where } k=2\pi HT \quad (2)$$

i.e., the volume of the slice is proportional to the average radius of the slice. In order to facilitate the estimation of the average radius of a short-axis slice in the phantom studies, the image gray scale was modified so that the hottest pixels were set to white. After appropriate adjustment of image contrast, a circle was then fitted to the white outline and the radius ($R$) of the circle noted.

In order to calculate the % IM in each short-axis slice, a circumferential profile was first generated for each slice by taking the maximum pixel count over every 6° arc. The curve profile was analyzed to obtain the peak, minimum, and mean values. The % IM was calculated as the percentage of segments whose counts were less than a fixed proportion (threshold value) of the peak curve profile value. Five threshold values were studied: These were 50%, 55%, 60%, 65%, and 70% of the peak curve profile value. The % IM in a given slice is then given by the equation

$$\%\ \text{IM}=100\times kRF \quad (3)$$

where $F$ represents the fraction of the curve profile below the threshold value. Hence, for a myocardium containing $n$ short-axis slices, total myocardial volume is given by the equation

$$\text{Myocardial volume}=k\sum_{i=1}^{n} R_i \quad (4)$$

and total volume of infarcted myocardium is given by the equation

$$\text{Total infarcted myocardium}=k\sum_{i=1}^{n} R_i F_i \quad (5)$$

Therefore,

$$\%\ \text{IM}=100\times \sum_{i=1}^{n} R_i F_i \Big/ \sum_{i=1}^{n} R_i \quad (6)$$

This technique requires that all myocardial slices be examined and the above equations applied.

*Measurement of percentage infarcted or jeopardized myocardium – three-slice technique.* A second simplified approach was based on the analysis of three representative myocardial slices, in the apical, midventricular, and basal sections. The apical slice was chosen by selecting the slice in which the left ventricular cavity was first visible and moving one slice further toward the base of the ventricle. The basal slice was chosen by selecting the slice in which a decrease in septal activity was first visualized and moving two slices further towards the apex of the ventricle. The midventricular slice was chosen half-way between the apical and basal slices. The radii of the apical ($R_A$), midventricular ($R_{MV}$), and basal ($R_B$) slices were determined as described above. The radii $R_B$ and $R_{MV}$ were then assumed to represent the average radii of hollow cylinders over the basal and midventricular portions of the heart. In order to model better the apical portion, this section was considered as a combination of a cylinder and a cone, each of equal length. The radius $R_A$ was considered to represent the average radius of both the hollow cylinder and the base of the hollow cone. The myocardial thickness was assumed to be equal throughout the heart. From standard geometry, this leads to a reduction of one-third in the contribution of the apical portion to total myocardial mass as compared with a cylindrical shape for the entire apical section. Myocardial volume was then given by the equation

$$\text{Myocardial volume}=kR_B+kR_{MV}+0.67kR_A \quad (7)$$

Following the generation of a circumferential profile and the application of the threshold value, the volume of the infarcted myocardium was then given by the equation

$$\text{IM}=kR_B F_B+kR_{MV} F_{MV}+0.67kR_A F_A \quad (8)$$

Therefore,

$$\%\ \text{IM}=100\times(R_B F_B+R_{MV} F_{MV}+0.67R_A F_A)/ \\ (R_B+R_{MV}+0.67R_A) \quad (9)$$

For large defects involving the entire apex, such as those present in studies 15 and 16 (Fig. 2), there are a number of additional problems in the measurement of % IM not discussed above. These are: (a) measurement of the short-axis slice ring radius at the apex in the absence of any apparent viable myocardial tissue and (b) determination of whether activity in the apical slice represents myocardial or background activity in cases whose peak profile counts in this slice are substantially less than those in other slices. From studies 15 and 16, it was found that when a large infarct involved the entire short-axis slice, the myocardium appeared as a cold circle. The approximate radius of this circle was measured and used as

a best estimate of the average radius of the myocardium. For both patient and phantom studies, inspection of the long-axis slices can be used to confirm the presence of an apical defect. The difficulty lies in determining the location of the boundary between infarcted and normal myocardium. To determine where viable myocardium begins in the short-axis slices, study 1 was analyzed to determine the lower threshold limit for normal myocardium. If peak counts in a slice fell below this threshold, the entire slice was considered to represent infarcted myocardium.

After calculation of % IM by the above equations for different count thresholds, the measured % IM was correlated with the true % IM by linear regression analysis.

## Results

Figure 3A gives the average circumferential profile counts for each short-axis slice from apex to base. Results are shown for a normal myocardium imaged using $^{99m}$Tc (study 1), $^{201}$Tl (study 19, 80 keV peak), and $^{201}$Tl (study 20, 80+170 keV peak). For each study, the profile with the highest average count has been normalized to 100. There was no significant difference between the three curves, indicating that differences in photon attenuation had little effect on the relative amplitude of the short-axis slices. Figure 3B shows the maximum to minimum variation in circumferential profile counts for each short-axis slice with $^{99m}$Tc. The greatest variation between maximum and minimum values in a given slice profile was 22% (slice 9), and in no slice did the peak profile count fall below 63% of the maximum for the entire study. Hence, a threshold value of 60% was set as the lower limit below which the entire short-axis slice was considered to represent infarcted myocardium. The arrows in Fig. 3B indicate the location of the apical, midventricular, and basal short-axis slices used in the three-slice technique.

Figure 4 compares the circumferential profiles generated from the midventricular slice in studies 11 and 21 (Fig. 2). These studies contained an identical inferobasal infarct but were imaged using $^{99m}$Tc and $^{201}$Tl. The $^{201}$Tl profile shows a higher minimum activity and a less steep slope at the boundary between normal and infarcted myocardium compared with the $^{99m}$Tc profile, suggesting a loss of contrast and resolution. For slices closer to the base of the heart, the angular width of the defect observed with $^{201}$Tl decreased by comparison with $^{99m}$Tc, and there was a more gradual transition from normal to infarcted myocardium. These results are consistent with the increased scatter present in a $^{201}$Tl image relative to a $^{99m}$Tc image (Budinger and Rollo 1977; Sorenson and Phelps 1987).

Table 1 presents the correlation between the true % IM and the % IM calculated by the three-slice technique and by analysis of all the short-axis slices (total slice technique) for studies 1–16. Irrespective of the threshold value employed, there was excellent correlation between the true % IM and measured % IM with $R^2 > 0.96$ in all cases.

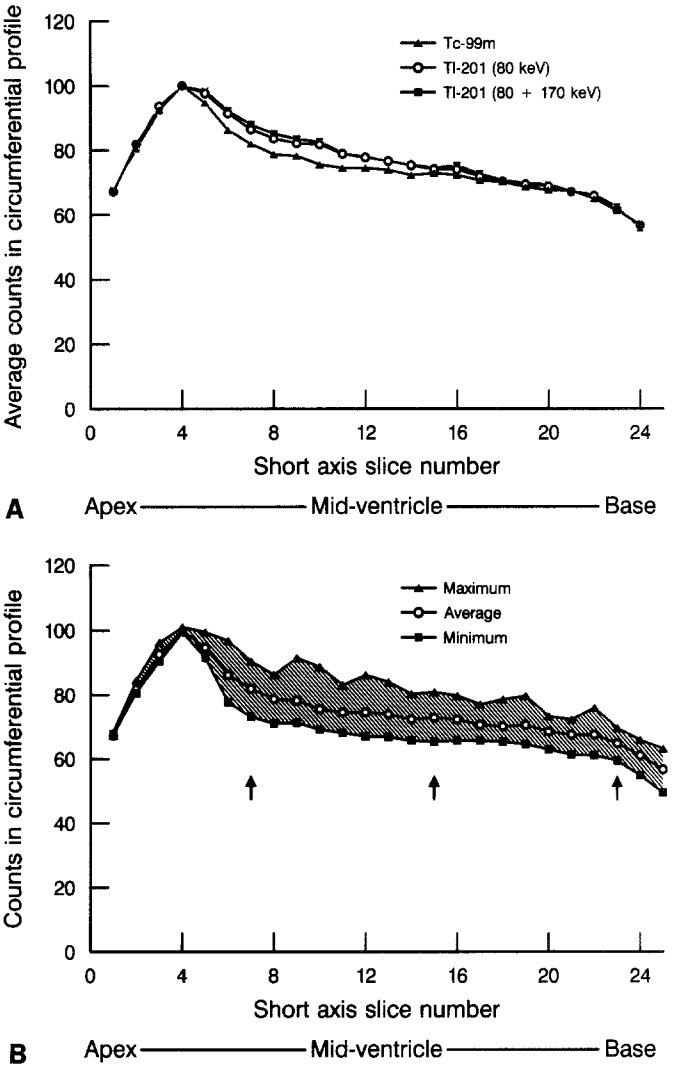


**Fig. 3.** **A** Average circumferential profile counts, in each slice, plotted as a function of slice number for a normal myocardium imaged with $^{99m}$Tc and $^{201}$Tl. Results have been normalized to the maximum value of average counts in all slices. **B** Maximum, minimum, and average circumferential profile counts plotted as a function of slice number for a normal myocardium imaged with $^{99m}$Tc. *Arrows* indicate the location of the apical, midventricular, and basal slices used with the three-slice technique. Results have been normalized as in **A**

Figure 5 plots the measured % IM against true % IM for the 55% threshold with the total slice technique (Fig. 5A) and for the 60% threshold with the three-slice technique (Fig. 5B). Although these figures illustrate the excellent correlation between true % IM and measured % IM, it can be seen that the measured % IM is dependent upon the location of the defect. For both techniques, myocardial defects placed in the anterior or anterolateral wall always gave a higher value than defects placed in the posterior wall or septum. From the seven sets of studies in which the defects were placed 180° apart in the myocardium (Fig. 2, studies 3–16), the average absolute difference in % IM was 3.8% (range 0%–9.4%) for the three-slice technique and 4.9% (range

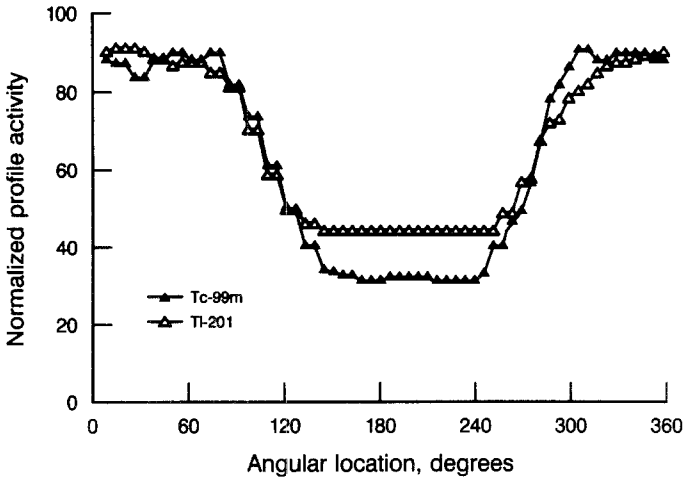


**Fig. 4.** Circumferential profiles generated from the midventricular slices of studies 11 and 21 (Fig. 2). Both studies contained an identical inferobasal infarct but were imaged with $^{99m}$Tc or $^{201}$Tl, respectively

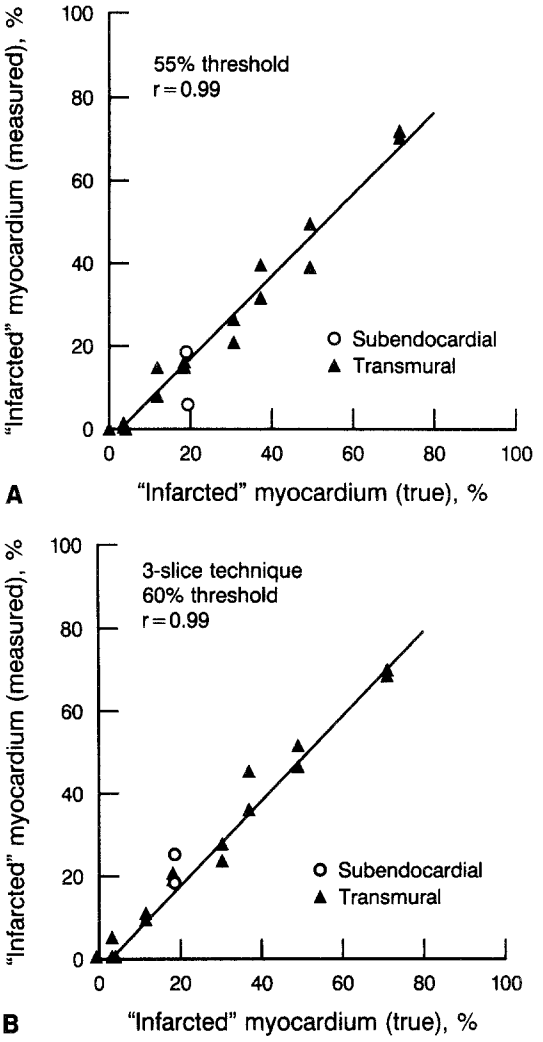


**Fig. 5A, B.** Relationship between true percentage "infarcted" myocardium and measured percentage "infarcted" myocardium for "transmural" infarcts obtained using **A** the total slice technique using a 55% threshold and **B** the three-slice technique with a 60% threshold. Lines represent the best fit

0.9%–10.5%) for the total slice technique. For the two studies containing subendocardial infarctions, the estimated infarct size was highly sensitive to the threshold value and to the location of the infarct (Fig. 5). For threshold values between 50% and 70%, the estimated infarct values ranged from 1.1% to 23.0% (total slice technique) and 2.6% to 24.1% (three-slice technique).

Measurement of the % IM by the three-slice technique is dependent upon a subjective selection of the appropriate apical and basal slices and upon a semiquantitative determination of the radii of the selected slices. All 15 studies (Fig. 2, 2–16) were re-analyzed in order to determine the sensitivity of the three-slice technique to both these variables. For the selection of the apical and basal slices, a slice variation of $\pm 1$ in slice number was evaluated and the % IM recalculated using a 60% threshold. The mean ($\pm$standard deviation) absolute difference in measured % IM was found to be 0.32% ($\pm$0.4%) and 1.57% ($\pm$2.5%) for the sets of slices closest and furthest from the midventricle, respectively. The largest error (8.2%, study 13) was caused by choosing the apical slice too close to the apex of the heart.

The effects of variation in determining the short-axis slice radius were investigated in a similar manner. For the 15 studies with "transmural" defects, all original measurements of short-axis radius were increased or decreased by one pixel and the % IM recalculated using Eq. (9). A uniform increase or decrease in ring radius

**Table 1.** Relationship between true percentage of infarcted myocardium (% IM) and measured % IM as a function of the curve profile threshold value for transmural infarctions. Results obtained by linear regression analysis

| Threshold (%) | Total slice technique | | | Three-slice technique | | |
|---|---|---|---|---|---|---|
| | Slope | Intercept | Correlation coefficient ($R^2$) | Slope | Intercept | Correlation coefficient ($R^2$) |
| 50 | 0.96 | −3.69 | 0.97 | 0.93 | −2.49 | 0.96 |
| 55 | 1.00 | −2.93 | 0.98 | 0.97 | −1.96 | 0.98 |
| 60 | 1.02 | −1.89 | 0.98 | 1.01 | −1.35 | 0.98 |
| 65 | 1.05 | −0.86 | 0.98 | 1.03 | −0.74 | 0.98 |
| 70 | 1.07 | 0.88 | 0.98 | 1.07 | −0.09 | 0.97 |

had minimal impact on the measurement of % IM with the three-slice technique. The mean (±standard deviation) absolute difference in % IM was 0.37% (±0.3%). The maximum absolute difference observed in any study was less than 1%.

## Discussion

Current radionuclide techniques for the measurement of infarct size are based upon analysis of $^{201}$Tl uptake in the myocardium. This radionuclide is not ideal for imaging purposes. There is a significant amount of Compton scatter inside the energy window with a consequential loss of image contrast and detail (Budinger and Rollo 1977; Sorenson and Phelps 1987). This presents difficulties in the detection and quantitation of infarcts present in deep cardiac structures such as the posterior ventricular wall. CT does not eliminate all these difficulties, as attenuation correction is not normally applied to cardiac structures due to the difficulty in accounting for the variable attenuation characteristics of muscle, lung, and bone tissue. Many of the above problems are significantly reduced with the use of $^{99m}$Tc instead of $^{201}$Tl.

In terms of photon attenuation, Fig. 3A shows that there is little difference between $^{99m}$Tc and $^{201}$Tl in our phantom model. This is to be expected since the attenuation characteristics for these radionuclides in soft tissue are similar (0.18 $cm^{-1}$ and 0.15 $cm^{-1}$ for $^{201}$Tl and $^{99m}$Tc, respectively). Figure 4 indicates that the important distinction between $^{99m}$Tc and $^{201}$Tl is the increased contribution of scatter to the $^{201}$Tl images. For a source 7 cm below the tissue surface, Compton scatter accounts for 62% of events falling within a 20% energy window at 80 keV, while at 140 keV, scatter represents only 35% of detected events (Anger 1967). The large increase in scatter with $^{201}$Tl results in a loss of contrast, making it more difficult to detect a small infarct or accurately define the boundaries of a large infarct (Fig. 4). This loss of contrast increases the difficulty in differentiating an infarct from the normal variation in $^{201}$Tl activity seen in CT short-axis slices of the myocardium. Hence, both the three-slice and total slice techniques are likely to prove less accurate when applied to $^{201}$Tl images.

We would expect the three-slice technique to be inherently less accurate than the total slice technique due to undersampling errors. However, from Table 1, it can be seen that for both techniques, a similar linear relationship exists between measured % IM and true % IM over the range of threshold values studied. The absence of any significant difference in the accuracy of the two techniques may be due to errors in the total slice technique. These errors arise in determining the exact location of the apex and in determining the apical contribution to total myocardial mass (partial volume effects). These effects are not present in the three-slice technique due to the method by which the apical slice is selected.

For the three-slice technique, a 57% threshold value was required to obtain an exact one-to-one correspondence with true % IM. In practice, thresholds between 50% and 65% gave similar estimates of % IM. In contrast with this result, many investigators have found that for $^{201}$Tl studies threshold definitions are critical to the estimation of infarct size (Holman et al. 1983; Johnson et al. 1987). From Fig. 5 it can be seen that the location of an infarct influences its apparent size. Presumably, this is due to increased scatter at depth which reduces the contrast of the lesion. For a given lesion, this "fill-in" of the cold area leads to a reduction in the estimation of % IM. We have not attempted to introduce a correction for this anatomic variation, as a vast series of experiments would be required to evaluate the full range of possible infarct sizes and locations. However, to a good approximation, translation of an infarct from a superficial to a deep location in the myocardium will lead to a 4% reduction in its apparent size.

Current nuclear medicine techniques for the quantitation of % IM are based almost exclusively upon the analysis of $^{201}$Tl tomographic studies. These techniques can be divided into two types – those using count thresholding followed by an edge detection algorithm to outline the boundaries of viable myocardium (Holman et al. 1983; Weiss et al. 1983) and those based upon circumferential profile analysis and comparison with a normal data base (Prigent et al. 1986; Tamaki et al. 1982). These techniques can accurately measure % IM using $^{201}$Tl and, with minor adaptations, could undoubtedly be applied to sestamibi Tc 99m studies with equal accuracy. While some investigators have developed sophisticated software to automate the analysis and computation of % IM (Weiss et al. 1983), in general these techniques require a considerable degree of operator intervention. Furthermore, the published techniques using circumferential profile analysis have the added disadvantage of requiring that a normal data base be generated. By comparison, the primary advantage of the three-slice technique is its simplicity. It does not require any specialized software other than the ability to generate a circumferential profile. Our results have shown that the estimate of percentage of myocardium "at risk" is relatively insensitive to the selection of slice number and the determination of ring diameter, provided that the operator is consistent in the technique. The technique is most sensitive to the selection of the apical slice, with the largest errors in estimation occurring with a slice chosen too close to the apex of the heart.

There are a number of assumptions and limitations in this study. The principle one is the assumption of relatively constant wall thickness, which is implicit in the formulae used to calculate infarct size. Variations in wall thickness between apex and base introduce an error into Eqns. (6) and (9) and hence into the estimation of myocardial mass. The contribution of each slice to the total myocardial mass is, to a good approximation, linearly dependent upon myocardial thickness. While this assumption is probably not correct in a setting of

chronic ischemic heart disease or cardiomyopathy, it should be valid in the acute infarct situation. This is the area in which we feel this technique has the greatest application.

Since we are using a static phantom, we cannot investigate the effects of wall motion on our results. The results of a study by Narahara et al. (1987) indicated that wall motion did not have a significant effect on the estimation of infarct size. However, that study was performed using $^{201}$Tl, and its poorer resolution may have masked any effects due to wall motion.

We have not fully assessed the accuracy of our technique in the measurement of subendocardial infarctions. From the results of studies 17 and 18 shown in Fig. 5, it is clear that the correlation between true and measured infarct size is not as good as for transmural infarctions. The estimate of subendocardial infarct size appears to be highly sensitive to the selected threshold value and to infarct location. Hence, these techniques may not be suitable for the estimation of subendocardial infarct size. A similar difficulty in the measurement of subendocardial infarct size has been observed by Narahara et al. (1987) using $^{201}$Tl.

The limitations of this technique are similar to those of $^{201}$Tl quantitative techniques. We have not investigated the effects of patient obesity or breast attenuation on the estimation of % IM. Both these factors will probably have a smaller but similar effect to that seen in $^{201}$Tl SPET studies. One of the main problems encountered with both $^{99m}$Tc and $^{201}$Tl SPET perfusion studies is the assessment of a large infarct located at the apex of the heart. Like previous investigators (Caldwell et al. 1984), we have assumed radial symmetry about the long axis of the left ventricle. However, our technique does have an advantage over other quantitative techniques in that it does not require the operator to outline the boundaries of the infarcted myocardium but simply to estimate the radius of the slice.

The lower limit of detection of infarcted myocardium with the three-slice technique would appear to be approximately 5%. Below this size, detection of an infarct is highly dependent upon its location in the myocardium (Fig. 5). This lower limit of % IM is similar to that found by many investigators using $^{201}$Tl quantitative techniques (Narahara et al. 1987; Caldwell et al. 1984).

In summary, we have described a simple three-slice technique for the assessment of the percentage of myocardium infarcted or at risk. The technique is intended for use with $^{99m}$Tc-labelled myocardial perfusion agents. It is not dependent upon any specialized computer software and only requires circumferential profile analysis of three representative short-axis slices of the myocardium. Our phantom results show that accurate quantitation of relative infarct size is possible. We are currently applying this technique to assess changes in myocardial perfusion, before and after treatment with intravenous tissue plasminogen activator, in patients with acute myocardial infarction (Gibbons et al. 1989).

## References


Anger HO (1967) Radioisotope cameras. In: Hine GJ (ed) Instrumentation in nuclear medicine. Academic Press, New York, pp 485–552

Budinger TF, Rollo FD (1977) Physics and instrumentation. Prog Cardiovasc Dis 20:19–53

Caldwell JH, Williams DL, Harp GD, Stratton JR, Ritchie JL (1984) Quantitation of size of relative myocardial perfusion defect by single photon emission computed tomography. Circulation 70:1048–1056

DeCoster PM, Melvin JA, Detry J, Brasseur LA, Beckers C, Col J (1985) Coronary artery reperfusion in acute myocardial infarction: assessment by pre- and post-intervention thallium-201 myocardial perfusion imaging. Am J Cardiol 55:889–895

Feiring AS, Johnson MR, Kioschos JM, Kirchner PT, Marcus ML, White CW (1987) The importance of the determination of the myocardial area at risk in the evaluation of the outcome of acute myocardial infarction in patients. Circulation 75:980–987

Gibbons RJ, Verani MS, Behrenbeck T, Pellikka PA, O'Connor MK, Mahmarian JJ, Wackers FJ (1989) Feasibility of technetium-99m-hexakis-2-methoxypropyl-isonitrile for the assessment of myocardial perfusion during and after acute myocardial infarction. Circulation 80:1277–1286

Granato JE, Watson DD, Flanagan TL, Gascho JA, Beller GA (1986) Myocardial thallium-201 kinetics during coronary occlusion and reperfusion: influence of method of reflow and timing of thallium-201 administration. Circulation 73:150–160

Holman BL, Moore SC, Shulkin PM, Kirsch CM, English RJ, Hill TC (1983) Quantitation of perfused myocardial mass using Tl-201 and emission computed tomography. Invest Radiol 18:322–326

Johnson LL, Lerrick KS, Coromilas J, Seldin DW, Esser PD, Zimmerman JM, Keller AM, Alderson PO, Bigger JT, Cannon PJ (1987) Measurement of infarct size and percentage myocardium infarcted in a dog preparation with single photon emission computed tomography, thallium-201, and indium 111-monoclonal antimyosin Fab. Circulation 76:181–190

Keyes JW, Brady TJ, Leonard PF, Svetkoff DB, Winter SM, Rogers WL, Rose EA (1981) Calculation of viable and infarcted myocardial mass from thallium-201 tomograms. J Nucl Med 22:339–343

Li QS, Frank TL, Franceschi D, Wagner HN, Becker LC (1988) Technetium-99m methoxyisobutyl isonitrile (RP 30) for quantification of myocardial ischemia and reperfusion in dogs. J Nucl Med 29:1539–1548

Narahara KA, Thompson CJ, Maublant CJ, Criley JM, Mena I (1987) Estimation of left ventricular mass in normal and infarcted canine hearts using thallium-201 SPET. J Nucl Med 28:1315–1321

Okada RD, Pohost GM (1984) The use of pre-intervention and post-intervention thallium imaging for assessing the early and late effects of experimental coronary arterial reperfusion in dogs. Circulation 69:1153–1160

Okada RD, Glover D, Gaffney T, Williams S (1988) Myocardial kinetics of technetium-99m-hexakis-2-methoxy-2-methylpropyl-isonitrile. Circulation 77:491–498

Prigent F, Maddahi J, Garcia EV, Satoh Y, Van Train K, Berman DS (1986) Quantification of myocardial infarct size by thallium-201 single photon emission computed tomography: experimental validation in the dog. Circulation 74:852–861

Ritchie JL, Davis KB, Williams DL, Caldwell J, Kennedy JW (1984) Global and regional left ventricular function and tomographic

radionuclide perfusion: the Western Washington Intracoronary Streptokinase in Myocardial Infarction Trial. Circulation 70:867–875

Schneider RM, Chu A, Akaishi M, Weintramb W, Morris K, Cobb F (1985) Left ventricular ejection fraction after acute coronary artery occlusion in dogs: relationship to the extent and site of myocardial infarction. Circulation 72:632–638

Sorensen JA, Phelps ME (1987) Physics in nuclear medicine. Grune and Stratton, New York, pp 221–229

Tamaki S, Nakajima H, Murakami T, Yui Y, Kambara H, Kadota K, Yoshida A, Kawai C, Tamaki N, Mukai T, Ishii Y, Torizuka K (1982) Estimation of infarct size by myocardial emission computed tomography with thallium-201 and its relation to creatinine kinase-MB release after myocardial infarction in man. Circulation 66:994–1001

Wackers FJ, Berman DS, Maddahi J, Watson DD, Beller GA, Strauss HW, Boucher CA, Picard M, Holman BL, Fridrich R, Inglese E, Delaloye B, Bischof-Delaloye A, Camin L, McKusick K (1989) Technetium-99m hexakis 2-methoxyisobutyl isonitrile: human biodistribution, dosimetry, safety, and preliminary comparison to thallium-201 for myocardial perfusion imaging. J Nucl Med 30:301–311

Weiss RJ, Buda AJ, Pasyk S, O'Neill WW, Keyes JW, Pitt B (1983) Noninvasive quantification of jeopardized myocardial mass in dogs using 2-dimensional echocardiography and thallium-201 tomography. Am J Cardiol 52:1340–1344